INSTITUT DE FRANCE
Académie des sciences

Comptes Rendus

Géoscience

Sciences de la Planète

Jean-Pierre Lorand and Sylvain Pont

Tl-rich pyrite and Sb-rich melnikovite in Montlouis pyrite veins (central armorican domain, Janze, Ille-et-Vilaine; France)

Volume 354 (2022), p. 303-317

Published online: 12 August 2022

https://doi.org/10.5802/crgeos.143

Les Comptes Rendus. Géoscience — Sciences de la Planète *sont membres du Centre Mersenne pour l'édition scientifique ouverte*
www.centre-mersenne.org
e-ISSN : 1778-7025

Comptes Rendus
Géoscience — Sciences de la Planète
2022, Vol. 354, p. 303-317
https://doi.org/10.5802/crgeos.143

Original Article — Geochemistry, cosmochemistry

Tl-rich pyrite and Sb-rich melnikovite in Montlouis pyrite veins (central armorican domain, Janze, Ille-et-Vilaine; France)

Jean-Pierre Lorand [*, a] **and Sylvain Pont** [b]

[a] Laboratoire de Planétologie et Géodynamique à Nantes (LPG) CNRS UMR 6112, Université de Nantes, Faculté des Sciences et Techniques 2 Rue de la Houssinière - BP 92208, 44322 NANTES CEDEX 3, France

[b] Institut de Minéralogie, de Physique des Matériaux, et de Cosmochimie (IMPMC) - Sorbonne Université- Muséum National d'Histoire Naturelle, UPMC Université Paris 06, CNRS UMR CNRS 7590, 61 rue Buffon, 75005 Paris, France

E-mails: jean-pierre.lorand@univ-nantes.fr (J.-P. Lorand), spont@mnhn.fr (S. Pont)

Abstract. Lower Ordovician sandstones of the "Grès Armoricain" formation in the Montlouis quarry near Janzé (Ille-et-Vilaine, France) display rare Fe-sulfide veins filled with a low-T (<300 °C) assemblage of pyrite, marcasite, "melnikovite", with trace amounts of galena and sphalerite. Pyrite occur as contorted cm-scale veins of columnar pyrite invading sandstones and as larger idiomorphic crystals coating vugs. It is usually overgrown by fibroradiated marcasite outer layer. Concentrically-layered spheroids of "melnikovite" separate pyrite from marcasite. This mineral sequence is consistent with crystallization from near-neutral, moderately reducing, H_2S-rich hydrothermal fluids evolving toward acidic conditions. Vug-hosted cm-sized pyrite cubes may be partly covered by a millimeter-thick fine-grained pyrite film. Unlike the other sulfide ores of the Central Armorican domain that carry Sb and Pb indices, trace element analyses identify As, Tl, Sb and Pb anomalies all distributed between Fe-sulfides, i.e. columnar vein pyrite (up to 1.0 wt% As), "melnikovite" (up to 5 wt% Sb), marcasite (up to 7600 ppm Pb) and fibrous pyrite overgrowths (up to 2060 ppm Tl). It is the first time that a Tl anomaly is reported in sulfide ores from the Armorican massif. A potential reservoir for Tl could be the altered dolerite body observed in the quarry.

Keywords. Hydrothermal pyrite, Variscan belt, Armorican massif, Epithermal orebodies, Thallium.
Manuscript received 6 April 2022, revised 1 July 2022, accepted 11 July 2022.

1. Introduction

Variscan orogen displays widespread evidence of hydrothermal processes [e.g. Boiron et al., 2003, Bouchot et al., 2005, Gasparrini et al., 2006]. Various evidences of Late Hercynian fluid circulations have been documented in Central/South Armorican tectonometamorphic domains of the Armorican Massif (i.e., thick quartz veins, Lemarchand et al. [2012]; kaolinite-dickite high-temperature clay mineral assemblage in kaolin deposits [Gaudin et al., 2020], and numerous sulfides orebodies carrying Pb, Zn, Sb and Au indices [Chauris and Marcoux, 1994]). Here we discuss a new Fe-sulfide occurrence

* Corresponding author.

of hydrothermal origin discovered in lower Ordovician sandstones at Montlouis, near Janzé (Ille-et-Vilaine), not far from several orebodies of the Central Armorican Domain (i.e. the abandoned mines of Pontpéan en Bruz near Rennes (Ille-et-Vilaine), La Touche-Vieux-Vy-sur-Couesnon (Ille-et-Vilaine) and Le Semnon (Ille-et-Vilaine) as well as the "Bois-de-la-Roche" quarry near Saint Aubin des Chateaux (Loire-Atlantique) [Chauris and Marcoux, 1994, Gloaguen et al., 2007, 2016, Pochon et al., 2016a,b, 2019]).

Sulfides were analysed with laser ablation-inductively coupled plasma mass spectrometry (LA-ICPMS) along with scanning electron microscopy to discuss element sourcing and partitioning between the various sulfide species. Except at Bois de la Roche near Saint Aubin des Chateaux, where electron microprobe analyses were performed on pyrite and associated sulfides [Gloaguen et al., 2007], it is the first time that Fe-sulfides involved in Armorican orebodies are analysed for trace elements. Our analyses identify some specific features compared with the other ores so far studied in the area such as Sb controlled by melnikovite and a Tl anomaly not yet recognized in that area. Montlouis is thus the first example of Tl anomaly in the Armorican massif and the third one in France after the unusual As–Sb–Tl paragenesis reported from Jas Roux (French Alps) [Johan et al., 1974], and geochemical indices documented in the Cévennes area [Aubague et al., 1982].

1.1. *Montlouis quarry and its pyrite veins*

The Montlouis quarry, a 320,000 m^2 open pit now operated by Lafarge Holcim™, is located near Janzé (Ille et Vilaine; France), 15 km to the north of Saint Aubin des Chateaux and 20 km to the southeast of Rennes, in the so-called "synclinorium of the south of Rennes" the Central Armorican Domain, (Figure 1). Here, folded paleozoic sediments rest unconformably on a neo-proterozoic basement made up from platform marine sediments [Gumiaux et al., 2004]. The Montlouis quarry is excavated within the Lower Ordovician sandstones of the "Grès Armoricain" formation. This detritic formation was deposited during an important marine transgression [Guillocheau and Rolet, 1982]. The quarry is encasted between two kilometre-scale N–S trending vertical faults [Trautmann et al., 1994]. This fault system was inherited from late Variscan deformation [Le Corre et al., 1991, Gumiaux et al., 2004, Pochon et al., 2018, 2019]. Sandstones are cross-cut by a body of deeply hydrothermally altered dolerite displaying sericitised plagioclase laths and skeletal Fe–Ti oxides (ilmenite, magnetite). Iron–Ti oxides are now replaced by rutile, pseudobrookite, and hematite and Ca-pyroxene by green amphibole, and epidote (pistachite), respectively. Similar rocks are widespread in the Central Armorican Domain [Trautmann et al., 1994] and the Armorican massif as a whole [Pochon et al., 2016a,b, 2019, and references therein].

The vein system discovered at Montlouis is poorly exposed over a few tens of square meters on the northern face of the quarry. It strikes along an overall N–S direction consistent with the late Variscan faulting system, although no reliable mean direction can be measured because of many discontinuities in the outcrop. Pyrite and the other Fe-sulfides identified (marcasite, melnikovite, galena, sphalerite) commonly occur as mm-scale to centimeter-thick veins showing no continuity on a larger scale, grading into sandstone breccias cemented by pyrite or diffuse impregnation of pyrite inside sandstones. Centimetric pyrite cubes are also present in larger vugs opened inside sandstones and coated with a quartz gangue. No gradation between the two modes of occurrences could be observed.

2. Analytical methods

Montlouis Fe-sulfides were studied with an Olympus BH-2 dual reflected-transmitted light microscope and a Tescan VEGA II LSU scanning electron microscope (SEM) operating in conventional (high-vacuum) mode, and equipped with an SD3 (Bruker) EDS detector (platform of electronic microscopes; Muséum National d'Histoire Naturelle Paris, France, MNHN). Major element concentrations were determined at 15 kV accelerating voltage with a PhiRoZ EDS standardless procedure. Accuracy was checked by repeated blind analyses of a natural troïlite-FeS (Del Norte County, USA) [Lorand et al., 2018].

LA-ICPMS analyses were done at the "Laboratoire de Planétologie et Géosciences; Nantes" using a Photon Machine Analyte G2 excimer laser (193 nm laser wavelength) coupled with a Varian 880 quadrupole ICP-MS through a cross-flow nebulizer. The largest pyrite crystals and their fibrous overgrowths were analysed on hand-picked crystals mounted in epoxy

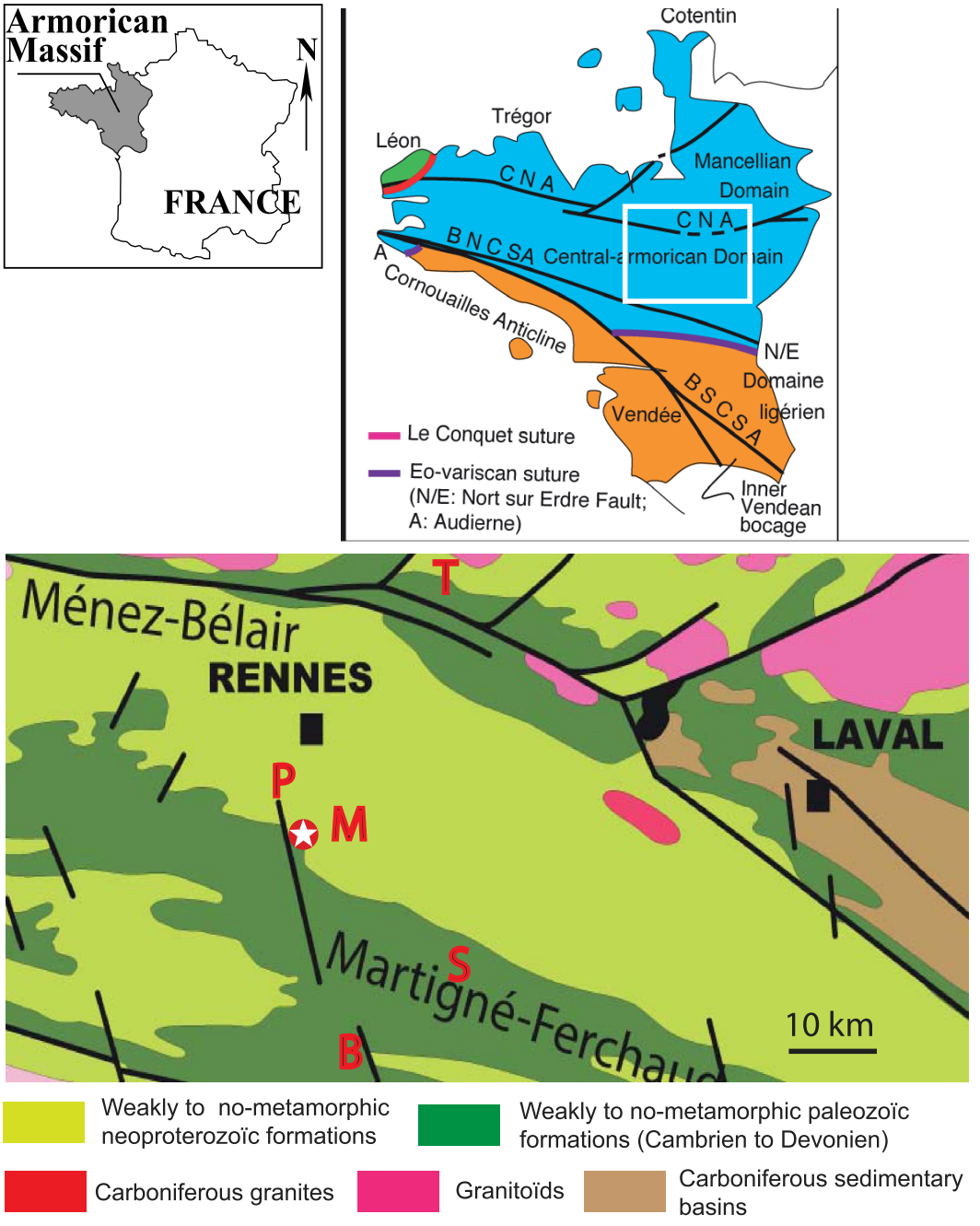

Figure 1. Location and geological setting of the Montlouis quarry (sketch map of the Variscan domains of the Armorican massif and geological background after Faure, 2021, https://planet-terre.ens-lyon.fr/article/chaine-varisque-France-2.xml redrawn and colorized after Le Corre et al., 1991). CNA North Armorican shear zone; BNCSA: Northern branch of the S. Armorican shear zone; BSCSA: Southern branch of the S. Armorican Shear Zone. T: La Touche-Vieux-Vy-Sur-Couesnon; P: Pontpéan-en-Bruz; M: Montlouis; S: Le Semnon-La Coefferie; B: Bois-de-la-Roche.

Table 1. Representative major element analyses of Montlouis Fe-sulfides

Mineral wt%	Py	Py	Mrc	Mrc	Ml	Ml	Ml
Fe	46.56	46.62	46.50	46.17	43.04	45.77	44.46
Sb	-	-	-	-	4.90	4.0	3.50
S	53.4	53.83	53.50	53.13	52.06	50.25	52.06
Total	99.96	100.45	100.0	99.30	100.0	100.02	99.92
Metal/sulfur atomic ratio	0.5	0.49	0.50	0.5	0.5	0.52	0.51

Py: pyrite; Mrc: marcasite; Ml: melnikovite.

resin. Marcasite and columnar pyrite were analysed *in-situ* on polished thick sections. Spot sizes for standards and samples were set to 81 μm. Repetition rate of 10 Hz using a laser output energy of 90 mJ with a 50% attenuator and 20× demagnification produces low fluences on the sample (<4 J/m^2).

Details on the analytical procedures were reported by Lorand et al. [2018, 2021]. The following isotopes were collected: ^{29}Si, ^{34}S, ^{51}V, ^{57}Fe, ^{59}Co, ^{60}Ni, ^{61}Ni, ^{63}Cu, ^{65}Cu, ^{66}Zn, ^{75}As, ^{77}Se, ^{95}Mo, ^{107}Ag, ^{118}Sn, ^{120}Sn, ^{121}Sb, ^{125}Te, ^{126}Te, ^{197}Au, ^{205}Tl, ^{207}Pb, ^{208}Pb and ^{209}Bi. Isotopes of each element to be analyzed, length of analysis (for spots) and dwell time were set to minimize potential interferences and maximize counting statistics—with overall mass sweep time kept to ~1 s. Major elements (S, Fe) were counted in the low-count rate mode to avoid saturation of detectors. External calibration was performed with synthetic standards MASS-1 [pressed Zn-sulfide powder; Wilson et al., 2002]. Each standard was analyzed twice every ten analyses to bracket sample measurements at the beginning and at the end of a single ablation run. Data reduction was done using Glitter™ software [Griffin et al., 2008]. Analyses of Fe-sulfides were quantified with S as internal standard, using 54 wt% as S concentration for pyrite and marcasite (Table 1) and 52 wt% S for melnicovite. Analytical precision was monitored by the repeated analysis of the sulfide standards yielding 10% RSD (relative standard deviation) for Au, Mn, Zn, Mo, Sb, Tl, Pb and Bi and 10–15% RSD for Co, Ni, Cu, Cd, Se and Ag.

3. Fe-sulfide mineralogy

Pyrite is by far the most abundant Fe-sulfide. Massive pyrite veins are made up from anhedral pyrite partly replaced by marcasite (Figure 2A). This latter may show up characteristic crystalline faces (i.e. (001), (110), (011) or (010)). Some pyrite veins show mineralogical zonation, often reported as banded textures in Fe-sulfide ores [e.g. Kucha and Stumpfl, 1992] (Figure 2B). The inner zone is composed of elongated pyrite crystals (columnar habit), terminated by cubic crystalline faces. The outer zone is occupied by fibroradiated marcasite. The contact zone between pyrite and marcasite is marked by botryoidal to colloform concentrically-layered spheroids up to 100 μm in diameter, looking like melnikovite, often reported as colloform pyrite [Ramdohr, 1980]. As usually reported in classic textbooks [Picot and Johan, 1977, Ramdohr, 1980], this compound appears much darker than pyrite in reflected light, tarnishing when stored in air (Figure 2C). It has lower reflectivity compared to coexisting pyrite [e.g. Kucha and Stumpfl, 1992] and display strong but false anisotropy in crossed-polarized reflected light. SEM picture of melnikovite reveals radial and concentric contraction cracks now filled with galena (Figure 2D). Back scattered electron images of concentrically-layered spheroids show inhomogeneous patchy zoning with some lighter areas characterizing heavier elements than Fe and S (Figure 3). This element is identified as Sb by X-ray scanning maps.

Vug-hosted euhedral pyrites usually display a darker core and a shiny periphery with weakly developed octaedral crystalline faces (111) (Figure 4A). The smallest isolated pyrite crystals that grew upon pyramidal quartz display more complex cubo-octaedral crystals shape combining (111) octaedral faces with (210) truncature. Pyrite cubes are occasionally coated with a mm-thick fine-grained pyrite overgrowths that pseudomorph the original cubes while sometimes developing its own crystalline faces (i.e. the octaedral faces on a perfect cube substratum (Figure 4B,C)).

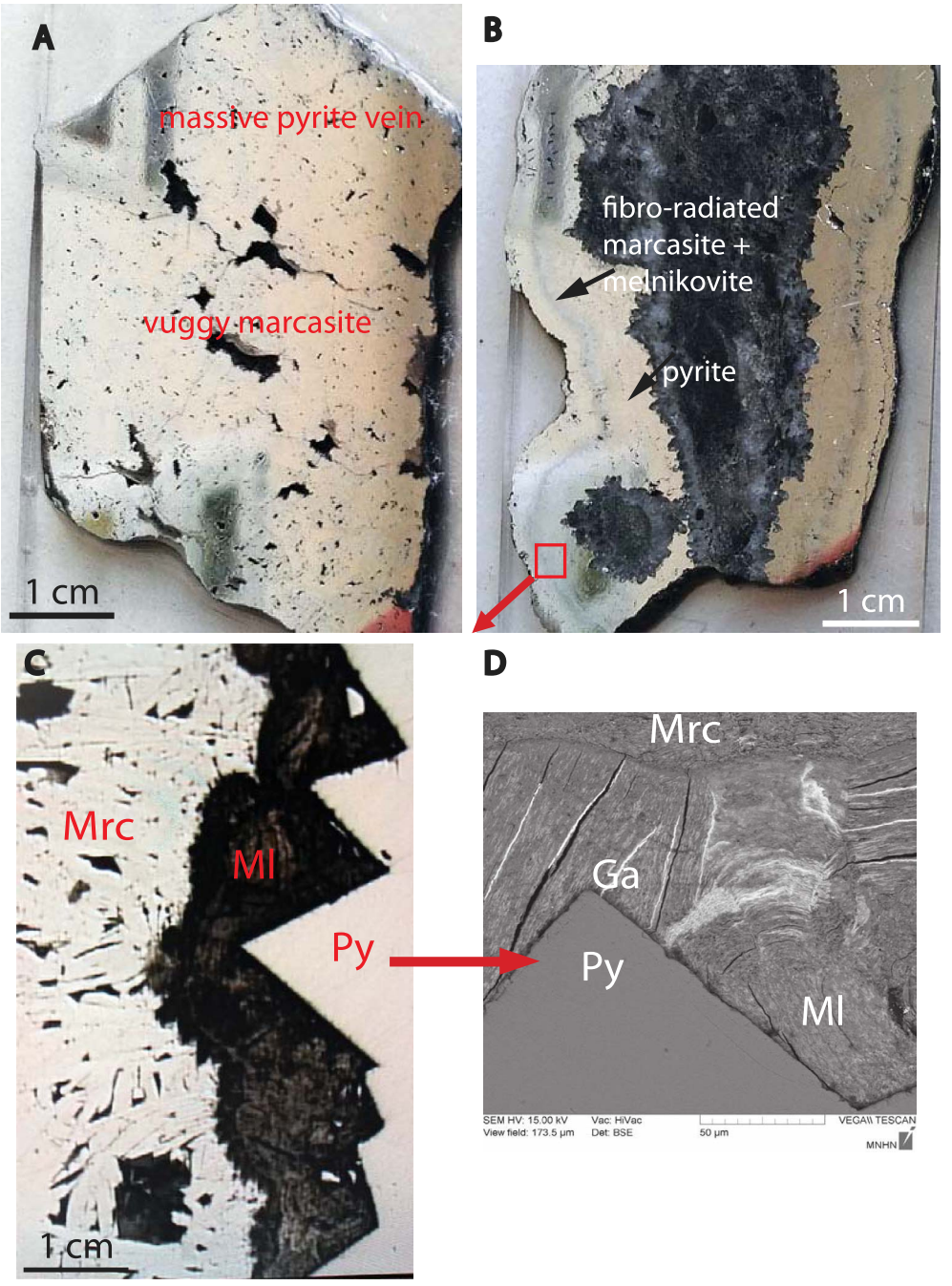

Figure 2. (A) polished thick section of a pyrite vein showing several vugs filled with marcasite (plane polariser reflected light). (B) Fe sulfide banded texture composed of an inner zone of elongated pyrite crystals (columnar habit), terminated by cubic crystalline faces and an outer zone of fibroradiated marcasite (plane polariser reflected light). (C) Detail of the contact zone between pyrite (Py) and marcasite (Mrc) showing botryoidal to colloform concentrically-layered spheroids of melnikovite (Ml) (plane polariser reflected light). (D) Back-scattered electron (BSE) image of melnikovite aggregates showing radial and concentric contraction cracks now filled with galena (Ga).

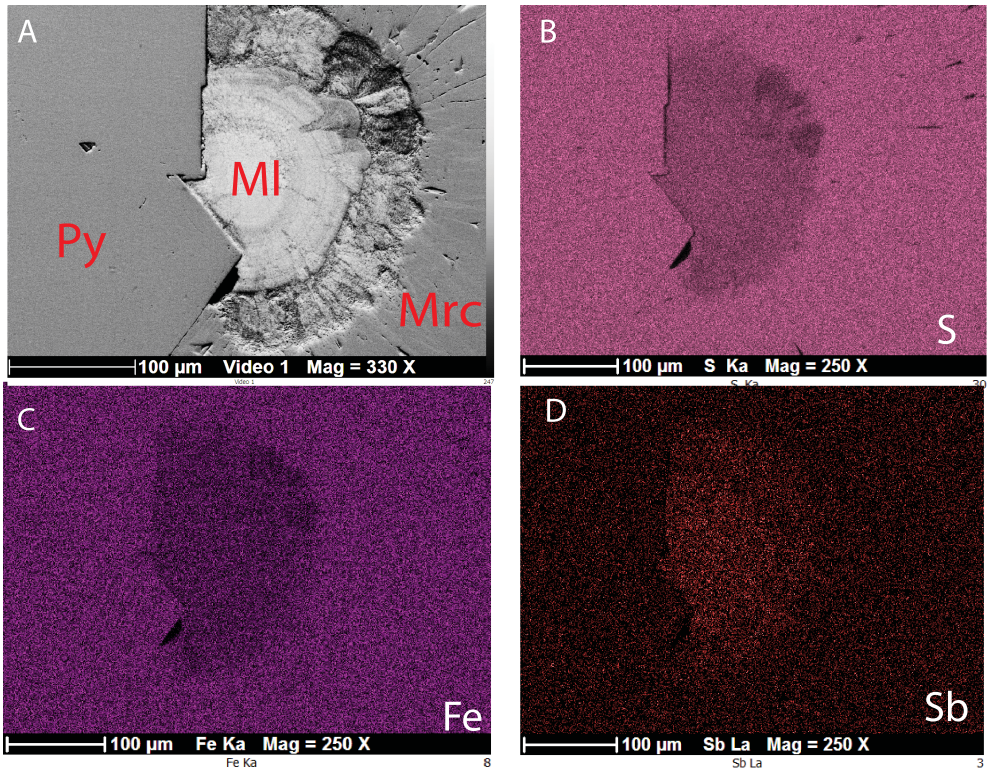

Figure 3. (A) BSE image of a melnikovite spheroïd (Ml) showing patchy zoning. Note the brightness of melnikovite compared to both pyrite (Py) and marcasite (Mrc). (B–D) X-ray maps showing attenuated Fe and S intensities compared to both pyrite and marcasite while Sb is identified as the heavy element of melnikovite.

This fine-grained pyrite overgrowth was observed to be isotropic under crossed-polariser reflected light. It is locally oxidized into goethite, thus getting a reddish-brown color (Figure 4D).

4. Major and trace element geochemistry

EDS analyses indicate closely similar mean atomic Fe/S ratios for pyrite, marcasite and melnikovite (Table 1). EDS spectra detected Fe, S and Sb as major elements in melnikovite, in agreement with back scattered electron images (BSE) and X-ray scanning maps (cf. Figure 3). Oxygen was systematically detected. According to Kucha et al. [1989], Kucha and Stumpfl [1992] and Kucha and Viaene [1993], natural melnikovite occurrences may be described as a variable mixture of disulfide and compounds with intermediate sulphur valencies. Sb-rich melnikovite seem to display distinct anisotropy as do As-rich variety [Ramdohr, 1980].

All three Fe-sulfides identified at Montlouis are nearly devoid of Au, Mo, Se In, Cd, Bi, Zn (Table 2). Their S/Se (55,000) is within the range of hydrothermal sulfides [5000–100,000; Luguet et al., 2004, Layton-Matthews et al., 2013, Queffurus and Barnes, 2015].

Vein-hosted columnar pyrite displays up to 952 ppm Ni, 155 ppm Co and 43.8 ppm Cu (Table 2). They are strongly As-enriched (up to 10,600 ppm) for low Sb (<317 ppm) and Pb (<510 ppm) contents and no specific Tl concentration anomalies (Figure 5A,B). Vug-hosted pyrite cubes and their fine-grained secondary pyrite overgrowth show much lower transition metal contents (<21 ppm Ni; <2 ppm Co). They also display moderate As-enrichment (<2754 ppm) and low Pb (<7.8 ppm), Sb (<38 ppm) and Tl (<3.4 ppm) contents (Figure 5A,B). Pyrite overgrowths are strongly Tl-enriched (up to 2033 ppm) and much lower in As (<20 ppm) than the other pyrite habits. Thallium positively correlates

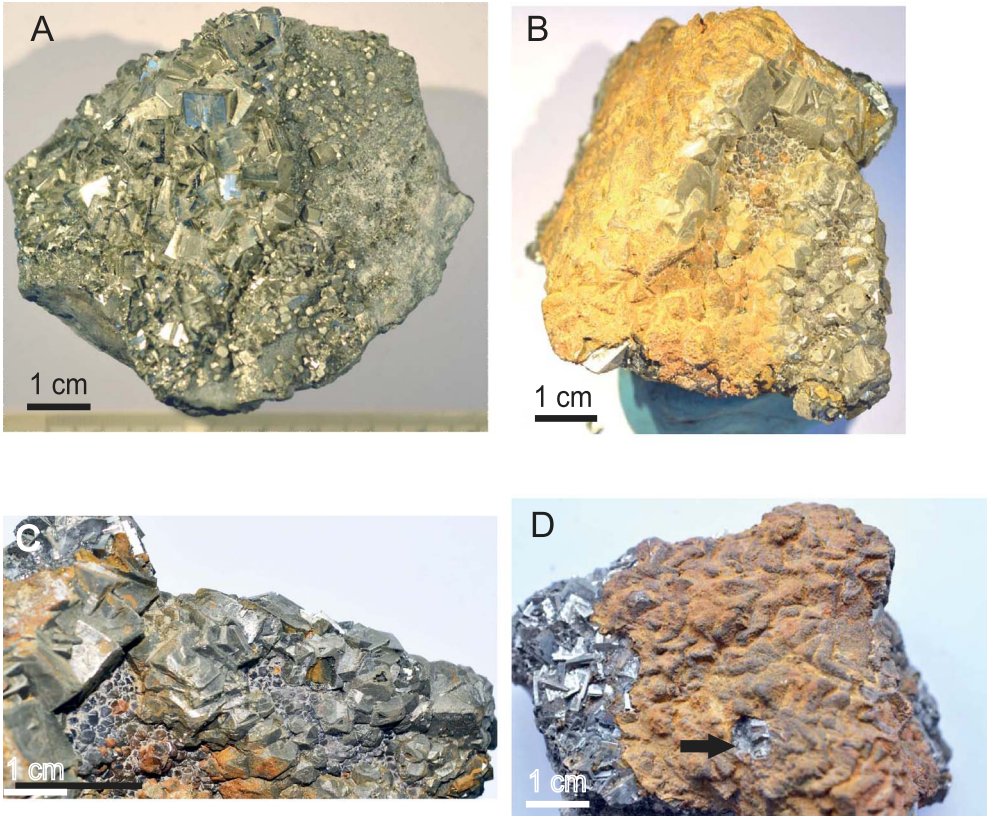

Figure 4. (A) Shiny cubic pyrite crystals sitting on pyramidal quartz and sandstone. (B) Pyrite cubes completely covered by fine-grained pyrite overgrowth, itself coated with clay minerals (bright yellow) (C) detail of specimen (B) showing the tarnished fine-grained pyrite overgrowth that pseudomorphs the original cubes. (D) Reddish-brown oxidized fine-grained pyrite overgrowth on cubic pyrite.

with Sb (<680 ppm). Nickel, Co and Cu are below detection limits (1 and 0.2 ppm, respectively) (Table 2).

Marcasite crystals show similar Ni and Co contents (up to 172 and 29 ppm, respectively) as their host columnar pyrite veinlet. Their strong Pb-enrichment (up to 7641 ppm) is noteworthy, as are their high Sb (<4000 ppm) and As contents (<1592 ppm). Lead positively correlates with Sb and Sb with As, respectively (Sb/As close to 3; Figure 5A). Thallium is detected, yet at much lower concentrations than in fine-grained pyrite overgrowths (<163 ppm).

Colloform melnikovite aggregates are As-depleted compared to their pyrite substratum (<700 ppm). Semi quantitative energy dispersive spectrometry (EDS) analyses indicate up to 5 wt% Sb (Table 1) while LA-ICPMS analyses yield lower but highly variable Sb contents (Sb < 11,400 ppm vs. 50,000 ppm; Figure 5A,B). Because it was larger than "melnikovite" spheroids, the laser beam intercepted composite marcasite-melnicovite aggregates rather than single-phase melnicovite, which diluted the actual Sb concentrations. Sb and As weakly correlate (Sb/As > 17; Figure 5A). A weak positive correlation seems to exist between Sb and Tl, yet melnikovite aggregates are only slightly enriched in Tl (<267 ppm) (Figure 5B).

5. Discussion

5.1. *Constraints from ore mineralogy*

Pyrite–marcasite–melnikovite assemblages are common low-temperature (<300 °C) hydrothermal

Table 2. Representative LA-ICPMS analyses of Montlouis Fe sulfides (ppm)

Element (ppm)	V	Co	Ni	Cu	Zn	Ga	As	Se	Mo	Ag	In	Sn	Sb	Au	Tl	Pb	Bi
Vein-hosted pyrite																	
Montl5-4	<0.032	7.76	58.66	43.25	<5.26	<0.095	2528.4	<1.11	0.03	0.5	0.05	<0.018	64.03	<0.003	4	68.2	0.022
Montl5-12	<0.039	0.82	<0.51	1.67	<6.56	<0.109	10,689.0	<1.40	0.08	<0.01	0.017	<0.023	26.05	0.05	0.28	4.8	0.003
Montl5-13	<0.043	158.2	952.1	20.88	<10.51	<0.121	3795.9	<1.45	0.25	0.12	0.005	<0.023	37.5	0.025	0.84	34.9	0.001
Montl3-15	<0.012	0.21	<0.29	2.61	<3.83	<0.063	1607.85	<0.81	<0.012	<0.005	0.0034	<0.015	45.9	0.003	1.5	1.7	0.001
Melnikovite																	
Montl3-2	<0.017	3.53	0.47	<0.59	<3.10	<0.048	714.9	3.1	1.04	<0.003	<0.0012	0.0119	11,369	0.002	140.7	11.85	<0.001
Montl3-6	<0.016	<0.060	<0.215	0.98	7.75	0.43	567.9	2.1	0.5	<0.004	<0.001	<0.011	10674.8	<0.001	267.05	16.4	<0.00
Montl3-8	0.04	1.04	<0.234	1.81	<3.62	<0.050	588.4	2.6	0.8	<0.004	<0.001	<0.014	8884.3	<0.001	106.95	1.58	0.012
Marcasite																	
Montl5-1	<0.029	2.75	32.9	<0.81	4.15	0.08	1084.6	<1.09	0.67	7.1	0.12	0.029	3107.6	0.017	63.6	7632.1	<0.001
Montl5-7	<0.023	3.57	77.5	3.33	8.58	<0.067	1020.5	<1.00	1.15	8.5	0.125	0.062	3890.2	<0.002	134.7	4941.9	<0.001
Montl5-10	<0.022	1.02	9.71	<1.16	<4.32	<0.066	810.5	<1.02	1.2	4.1	0.06	0.024	3383	<0.002	71.75	3843.7	0.007
Montl5-17	<0.032	2.02	51.67	2.07	<6.24	<0.093	981.5	<1.25	0.68	2.7	0.05	0.053	2734.5	<0.003	40.2	1949	<0.001
Vug-hosted pyrite cubes																	
Montl-2-1	0.041	0.37	<0.64	5.65	<6.50	<0.127	1721.8	<1.80	0.165	0.111	<0.002	<0.036	30.3	<0.002	1.9	4.78	0.03
Montl-2-3	0.056	0.41	<0.65	5	4.52	<0.106	1375.5	<1.41	0.212	0.142	0.002	0.04	26.5	<0.003	1.6	4.15	<0.002
Montl-4-1	<0.049	<0.189	<0.87	<5.84	<15.41	<0.185	79.3	<0.12	<0.036	<0.014	<0.002	<0.050	11.14	<0.004	0.4	1.4	<0.002
Montl-10-1	<0.067	<0.28	<1.67	<5.12	<12.44	<0.184	225.5	<3.47	<0.048	3.75	<0.002	0.045	3.63	0.023	0.04	0.44	0.015
Fine-grained pyrite overgrowth																	
Montl-5-3	<0.029	<0.119	<0.71	2.84	<7.20	<0.093	12.6	<1.62	1.124	0.0312	<0.001	<0.024	492.2	<0.002	2032.95	32.9	0.002
Montl-6-1	<0.030	<0.116	1.03	<2.47	8.91	<0.087	20.1	<1.58	1.11	0.038	0.001	<0.023	680.9	<0.002	1920.4	70.9	0.005
Montl-6-3	<0.031	<0.127	<0.76	<3.20	<7.22	<0.090	18.1	<1.72	0.967	0.0196	<0.001	<0.023	603.8	0.009	1797.37	60.1	<0.001
Montl-8-3	<0.043	<0.163	<0.96	3.15	<9.68	<0.102	2.1	<2.08	1.09	0.0187	<0.001	<0.024	438.7	<0.002	1179.6	0.47	0.003
Montl-9-1	<0.046	<0.189	1.36	6.47	<9.58	0.21	2.75	<2.41	1.043	0.152	<0.002	<0.028	173.5	<0.002	295.4	4.51	0.045

mineralisations [Gemmell and Simmons, 2007]. Ore mineralogy of Montlouis mineralization suggests that pyrite precipitated first as large cubes and massive veins after quartz, then followed by melnikovite/marcasite and/or fibrous pyrite overgrowths. Pyrite ore-forming solutions typically show near-neutral pH, are moderately reducing, and contain significant amounts of H_2S and minor CO_2 [Wang et al., 2010, Gartman and Luther, 2013]. The largest veins and cubic crystals precipitated under near equilibrium, under a low degree of supersaturation in the fluids because cubic crystals and cubo-octahedral form spontaneously from H_2S fluids, without requiring a high degree of supersaturation because cubes have the lowest Gibbs free energy of formation and their {100} faces have the lowest atom density and the highest growth rates [Murowchick and Barnes, 1986, 1987, Keith et al., 2016, Rickard and Luther III, 2007, Wang et al., 2010, Barnard and Russo, 2007]. The octahedral {111} faces that rarely appear in the smallest pyrite cubes have higher atom density, and thus slower growth rates. The sequence pyrite–marcasite can be ascribed to decreasing pH during ore precipitation. Pyrite indicates maximum pH < 9, and log fO_2 −36 to −30 at 300 °C [Vaughan and Craig, 1978] while octahedral pyrite may indicate local excursion of pH to 11, stabilizing polysulfide species (S_n^{2-}) [Wang et al., 2010, Gartman and Luther, 2013]. Marcasite was reported to form only at pH < 4 (<5–6) and in presence of elemental sulfur [Murowchick and Barnes, 1987, Schoonen and Barnes, 1991, Rickard and Luther III, 2007]. This sequence of decreasing pH is supported by kaolinite infilling of pyrite vugs [pH < 6; cf. Sher et al., 2013].

Melnikovite was often interpreted as bertierite ($FeSb_2S_4$) replacement product [Picot and Johan, 1977, Achimovičová and Balaz, 2008]. This interpretation could account for the high Sb content measured in Montlouis melnikovite. However, as it predates marcasite, a primary origin is more likely for melnikovite: the contraction cracks testify to process of reduction connected with a reduction in volume. A similar primary origin was postulated for mel-

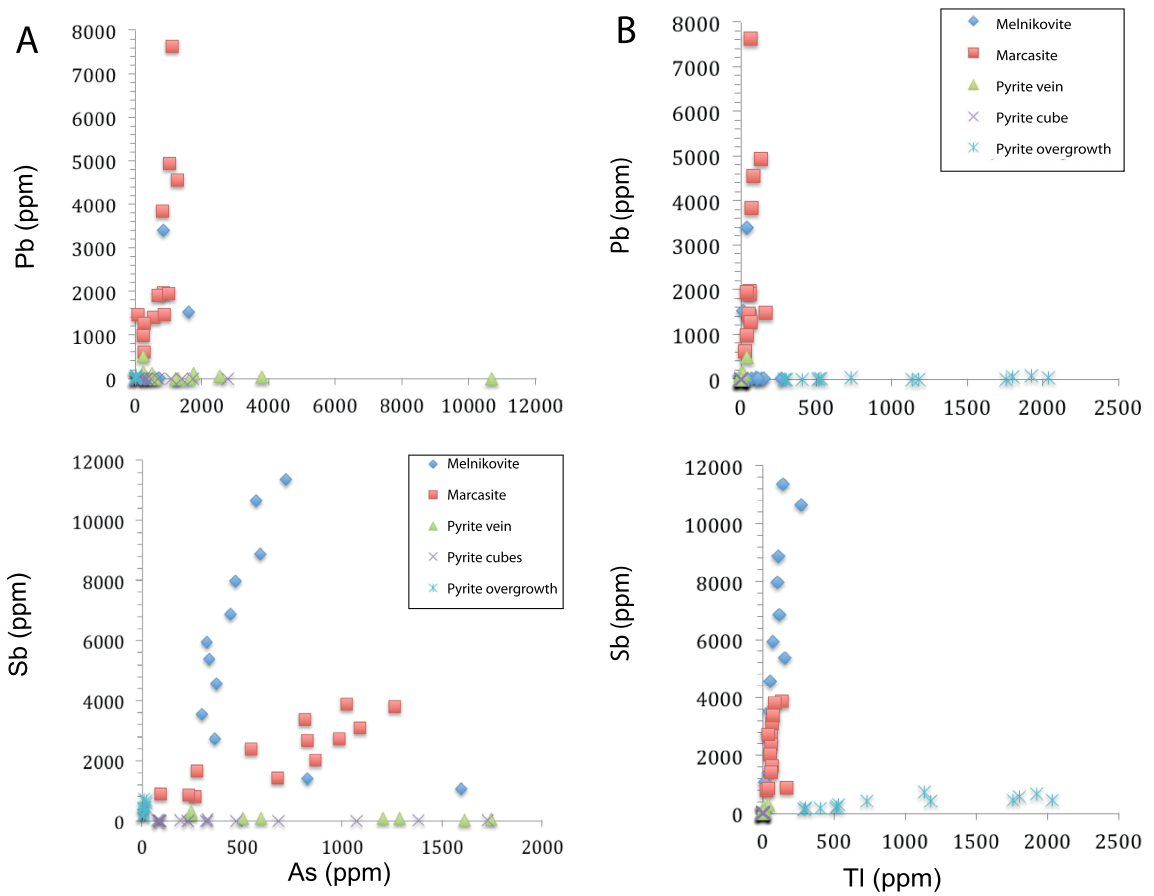

Figure 5. (A, B) Binary plots of trace elements for Montlouis Fe-sulfides.

nikovite by Kucha and Stumpfl [1992] in Bleiberg banded pyrite structure (Austria); they concluded that such compounds with mixed S valencies can be the natural precursor for banded sulfides formed below 250–300 °C. Thiosulfates species are unstable in acidic environments and soluble in water. The paragenetic succession pyrite–melnikovite–marcasite observed in the Montlouis ore is therefore consistent with the decreasing pH of solutions carrying Fe and S, as discussed above. It also suggests input of oxidized S alternating with reduced S that reflect flutuation in redox potentials. According to Kucha et al. [1989] both Pb and Sb may decrease the solubility of thiocomplexes, thus precipitating these latter as melnikovite. This process could account for the intimate associated between galena and Sb-rich melnikovite in Montlouis Fe sulfide ores.

5.2. *Trace element constraints*

As shown by SEM analyses and time-integrated laser-ablation analyses, submicroscopic inclusions of sphalerite and galena are very scarce in Montlouis Fe-sulfides and no other mineral inclusion were detected in the three Fe-sulfides. Trace element incorporation likely operated mainly by stoichiometric and non-stoichiometric substitutions. Among elements entering pyrite as stoichiometric substitution, Ni, Co, Se are of specific interest as they are temperature-sensitive elements, being typically enriched in sulfides that precipitate at high temperatures [e.g. Abraitis et al., 2004, Keith et al., 2016]. The Ni concentration level of Montlouis columnar pyrite (corresponding to 0.1 mol.% NiS_2 at best) is consistent with the low-temperature origin of this epither-

mal deposit (<300 °C). At 500 °C, pyrite can dissolve up 10–11 mol.% NiS_2; [Vaughan and Craig, 1978, Lorand et al., 2018]. At first sight, the extremely low Se concentrations in Montlouis pyrites also support a low-T formation because Se is a low-solubility elements that precipitate at high T (>350 °C) in terrestrial active hydrothermal vents and is commonly enriched in corresponding high-T sulfides [Keith et al., 2016, Maslennikov et al., 2020]. Taken as a whole, all three Fe-sulfides display extremely low Se/As ratio, as expected for low-temperature hydrothermal sulfides [Reich et al., 2013].

Trace element concentrations bear evidence for a late stage enrichment in Sb, Pb and Tl in the Montlouis orebodes, i.e. marcasite for Pb, fine-grained pyrite overgrowth for Tl and melnikovite for Sb. The LA ICPMS time-resolved down-hole ablation profiles of marcasite, melnikovite and fibrous pyrite were smooth indicating that Tl, Sb and Pb are dissolved in the sulfide matrix, or occur as homogeneously distributed nanoinclusions. The fact that Tl and Sb moderately correlate in the fine-grained pyrite coating the largest pyrite cubes suggests that the coupled substitution of $Tl^{+} + (As, Sb)^{3+}$ for $2Fe^{2+}$ documented by D'Orazio et al. [2017] also operated in Montlouis pyrite. However, Tl is bigger than Fe, Ni and Co. Rather than mineral/fluid equilibrium partitioning, a kinetic effect could explain why Tl was concentrated in fibrous pyrite aggregates rather than in more massive pyrite. Duchesne et al. [1983] pointed out that Tl is preferentially enriched in minerals presenting a colloform texture. Likewise, Maslennikov et al. [2020] documented preferential concentrations of Tl in fine-grained pyrite and marcasite precipitated from mid- and low-temperature fluids, the contents of these elements declining with increasing crystal size. George et al. [2019] also suggested that Tl could occur in structural defects in pyrite. Fine-grained pyrite overgrowth textures may therefore indicate disequilibrium conditions resulting from rapid crystallization, perhaps due to mixing between hydrothermal fluid batches [Berkenbosch et al., 2019]. This sequence of event is not uncommon in low-temperature hydrothermal ores: colloform, radiated, and oscillatory-zoned marcasite along with Tl-rich pyrite were documented in late disseminated sulfides or the outer walls of volcanic-hosted mineralization associated with vent chimneys [Smith and Carson, 1977, Sobbot et al., 1987, Maslennikov et al., 2020, and references therein]. These latter authors describe sooty colloform marcasite becoming black which looks like melnikovite.

5.3. *Montlouis Fe-sulfide ores and Central Armorican variscan mineralizations*

There is little doubt that the Montlouis ore veins belong to the same Variscan mineralized province as the Pb–Zn–Sb–Au orebodies hosted in the Central Armorican Domain, not far from Montlouis. All of these orebodies appear to be driven by faults of broadly NW–SE direction which were recognized at La Touche (Vieux-Vy-sur-Couesnon) [Tanon, 1961, unpublished report], Le Semnon Sb–Au orebodies [northern limb of the Chateaubriant anticline; Pochon et al., 2016a, 2019] and the Bois-de-la-Roche quarry (Saint Aubin des Chateaux; southern limb of the Châteaubriant anticline) [Gloaguen et al., 2007]. Dolerites that are spatially associated with Montlouis Fe sulfide veins are also present in the Pontpéan Pb–(Zn) ore [Lodin, 1908, Moussu and Prouhet, 1957, unpublished report] and as dike swarms at Le Semnon [Pochon et al., 2016b]. Some mineralogical similarities can also be recognized. The La-Touche orebody consists in massive pyrite–marcasite–melnikovite–pyrrhotite following Ag-rich sphalerite and galena in the paragenetic sequence [Chauris, 1977, Pillard et al., 1985]. At Pontpéan a pyrite–sphalerite–galena ore is overgrown by pyrrhotite, itself replaced by botryoidal marcasite spheroids (or melnikovite ?) with fibroradiated texture [Moussu and Prouhet, 1957, unpublished report; Chauris, 1977]. At Le Semnon, pyrite and marcasite replace an early Fe–As–(Au) ore stage consisting of arsenopyrite [with numerous inclusions of Sb-sulfosalts; Gloaguen et al., 2016, Pochon et al., 2016a] while in the Bois-de-la-Roche quarry, the oolitic ironstone horizons (OIH) intercalated in Lower Ordovician sandstones is replaced by stratoid pyrite lenticular bodies with euhedral arsenopyrite inclusions and marcasite (locally up to 50 vol.%). Pyrite is also expressed in a second hydrothermal event with quartz, chalcopyrite, sphalerite and galena assemblage [Gloaguen et al., 2007].

The Montlouis orebodies display a sequence of geochemical anomalies that are also consistent with those reported for the Sb-ores i.e. an As positive

anomaly associated with the earliest pyrite that contains similar As concentration levels as in Bois-de-la-Roche type-1 pyrite [Gloaguen et al., 2007] while the latest sulfides (marcasite, melnikovite and fibrous pyrite overgrowths) are characterized by overall increase of Pb and Sb contents. Stibnite is a late precipitate compared with pyrite–melnikovite–marcasite in the La Touche orebody [Chauris, 1977] as are berthierite and the main Sb mineralization at Le Semnon [Gloaguen et al., 2016, Pochon et al., 2016a, 2018] and Pb–Sb–Au-sulfosalts in the Bois-de-la-Roche quarry [Gloaguen et al., 2007]. However, there are major differences compared to Le Semnon or Bois de La Roche deposits such as the lack of pyrrhotite and arsenopyrite, while neither Sb sulfides/sulfosalts nor native antimony or gold have been identified so far at Montlouis. Compared to Pontpéan and Vieux-Vy sur Couesnon ores, the scarcity of Pb–Zn sulfides (galena, sphalerite) in Monlouis veins is noteworthy.

The Montlouis Fe-sulfide veins thus provide a further evidence for a large-scale Sb mineralizing peak in the southeastern part of the Central Armorican Domain. Pochon et al. [2017] concluded that Sb was sourced in the 360 Ma-old alkaline continental flood basalts that produced dolerites dikes. This origin may also pertain to the Montlouis pyritic veins which are spatially associated with a doleritic dike. Moreover, the high Ni/Co ratio of columnar pyrite points to contribution from hydrothermally altered mafic minerals such as olivine or pyroxene that are present in altered dolerite [Kaasalainen et al., 2015, Patten et al., 2016, and references therein]. With this interpretation, an upper age of ca 360 Ma, the age of magmatic crystallization of dolerites, can be inferred for Montlouis Fe sulfide veins. These latter, however, are likely younger. According to Pochon et al. [2017], hydrothermal alteration that liberated Sb involved a complex two-stage model postdating magmatic crystallization of dolerites. Moreover, N160° E-trending faults that control Sb–Au ores were active from the Early Carboniferous to the Early Permian [Pochon et al., 2019]. Most Variscan hydrothermal mineralizations were dated between 335 and 315 Ma [e.g. Chauris and Marcoux, 1994].

The thallium concentration of Montlouis pyrite is the most distinctive feature compared to the other Pb–Sb–Au ores of the Central Armorican domain. It is the first Tl anomaly reported in the Armorican massif and the third one in France after the unusual As–Sb–Tl paragenesis from Jas Roux (French Alps) [Johan et al., 1974], and geochemical indices of Tl-rich marcasite documented in sedimentary Mesozoïc deposits from the Cevennes [Aubague et al., 1982]. In the Jas Roux ore, like in Montlouis pyrite, Tl precipitates at the latest stage of the ore forming event(s), namely after stibnite [Johan et al., 1974]. Thallium, like Sb and Pb has properties of highly volatile, fluid-mobile elements that are easily transported by hydrothermal fluids [Ryan and Chauvel, 2014, and references therein].

A potential source for Tl is the altered dolerite body that is assumed to have provided Ni, Co and Sb to Montlouis Fe-sulfides. Thallium shows lithophile behavior in magmatic rocks and behaves as a highly incompatible element during magmatic differentiation, correlating with K, Rb, Sr, and Ba [Shah et al., 1994, Rader et al., 2018, Calderoni et al., 1983]. Therefore altered feldspar and micas are potential reservoirs for Tl [D'Orazio et al., 2017]. The elemental association of Tl, Sb, and As is also known worldwide in stratiform basin-hosted sulfide deposits (e.g. Carlin-type deposits Nevada, USA) [D'Orazio et al., 2017, and references therein] where pyrite can incorporate extremely high Tl contents (up to 35,000 ppm) as reported by Zhou et al. [2005] for the Xiangquan deposit (China). It is worth noting that, like Montlouis Fe-sulfides, the few Tl-bearing orebodies documented so far in France are hosted in sedimentary rocks, either dolostones or detrital rocks [Johan et al., 1974, Aubague et al., 1982] as is the Vedrin deposits (Belgium) that shows Tl-rich fibrous marcasite (6800 ppm Tl) [Duchesne et al., 1983]. If a sedimentary component was involved in Montlouis pyrite, then it has to be searched for in Middle ordovician slatty schists overlying ordovician sandstones of the "Grès Armoricain" formation. These black schists show compositional features of anoxic shales which are known to be strongly enriched in heavy metals due to organic material and microbial activities [e.g. Brumsack, 2006, Algeo and Maynard, 2004]. One may speculate that this sedimentary source was locally tapped by downgoing hydrothermal fluids. As discussed before, a mixing process between different hydrothermal fluid batches may account for the fine-grained pyrite overgrowth textures reflecting disequilibrium conditions. It is also consistent with the decoupling between Tl and Sb, Pb and As in that fine-grained pyrite (Figure 5B).

6. Conclusion

The Montlouis ores belong to the Variscan mineralizing event that led to Pb–Zn–Sb–Au orebodies hosted in the Central Armorican Domain. Pyrite veins display low-temperature (<300 °C) mineral assemblages of pyrite, marcasite, "melnikovite" with trace amount of galena and sphalerite. This mineral sequence is consistent with crystallization from near-neutral, moderately reducing, H_2S-rich hydrothermal fluids evolving toward acidic conditions.

Stibnite, Cu sulfides and Pb–Sb sulfosalts are absent, unlike the other Sb–Pb ores of the Central Armorican domain. Trace element analyses identify As, Tl, Sb and Pb anomalies carried by Fe-sulfides, i.e. columnar vein pyrite (up to 1.0 wt% As), "melnikovite" (up to 5 wt% Sb), marcasite (up to 7600 ppm Pb) and fibrous pyrite overgrowths (up to 2060 ppm Tl). Potential reservoirs for Sb and Tl could be altered dolerite body observed in the quarry, or the middle Ordovician Angers-Traveusot black schists.

Conflicts of interest

Authors have no conflict of interest to declare.

Acknowledgements

We thank Jean-Luc Bourguet (Lafarge Holcim) for providing access to the Montlouis quarry and his help during collection of the samples studied. We thank Laurent Lenta (LPG) for preparing the polished sections and Carole La (LPG) for her help during Laser-Ablation inductively coupled-mass spectrometry analyses. The present version of the paper was greatly improved through thorough reviews of Yves Moëlo and an anonymous reviewers, and careful reading of Eric Marcoux and associate editor Michel Faure. Their contributions are warmly acknowledged. Financial support was provided by the Centre National de la Recherche Scientifique (CNRS-UMR 6112).

References

Abraitis, P. K., Pattrick, R. A. D., and Vaughan, D. J. (2004). Variations in the compositional, textural and electrical properties of natural pyrite: a review. *Int. J. Miner. Process.*, 74, 41–59.

Achimovičová, M. and Balaz, P. (2008). Kinetics of the leaching of mechanically activated berthierite, boulangerite and franckeite. *Phys. Chem. Miner.*, 35, 95–101.

Algeo, T. J. and Maynard, J. B. (2004). Trace-element behavior and redox facies in core shales of Upper Pennsylvanian Kansas-type cyclothems. *Chem. Geol.*, 206, 289–318.

Aubague, M., L'Homer, A., and Sureau, J. F. (1982). Gites Pb–Zn liés aux strates en environnement dolomitique (Bois-Madame, La Croix-de-Paillières, Figeac). *Chron. de la Rech. Minière*, 466, 41–50.

Barnard, A. S. and Russo, S. P. (2007). Shape and thermodynamic stability of pyrite FeS_2 nanocrystals and nanorods. *J. Phys. Chem.*, 111, 11742–11746.

Berkenbosch, H. A., de Ronde, C. E. J., Ryan, C. G., McNeill, A. W., Howard, D. L., and Gemmell, J. B. (2019). Trace element mapping of Copper- and Zinc-Rich Black Smoker Chimneys from Brothers Volcano, Kermadec Arc, using synchrotron radiation XFM and LA-ICP-MS. *Econ. Geol.*, 114, 67–92.

Boiron, M. C., Cathelineau, M., Banks, D. A., Fourcade, S., and Vallance, J. (2003). Mixing of metamorphic and surficial fluids during the uplift of the Hercynian upper crust: consequences for gold deposition. *Chem. Geol.*, 194, 119–141.

Bouchot, V., Ledru, P., Lerouge, C., Lescuyer, J.-L., and Milesi, J.-P. (2005). Late Variscan mineralizing systems related to orogenic processes: The French Massif central. *Ore Geol. Rev.*, 27, 169–197.

Brumsack, H.-J. (2006). The trace metal content of recent organic carbon-rich sediments: implications for Cretaceous black shale formation. *Palaeogeogr. Palaeoclimatol. Palaeoecol.*, 232, 344–361.

Calderoni, G., Giannetti, B., and Masi, U. (1983). Abundance and behavior of thallium in the K-alkaline rocks from the Roccamonfina volcanic (Campania, Southern Italy). *Chem. Geol.*, 38, 239–253.

Chauris, L. (1977). Les associations paragénétiques dans la métallogénie varisque du Massif Armoricain. *Mineral. Deposit.*, 12, 353–371.

Chauris, L. and Marcoux, E. (1994). Metallogeny of the Armorican Massif. In Chantraine, J., Rolet, J., Santallier, D. S., Pique, A., and Keppie, J. D., editors, *Pre-Mesozoic Geology in France and Related Areas, IGCP-Project 233*, pages 243–264. Springer, Berlin,

Heidelberg.

D'Orazio, M., Biagioni, C., Dini, A., and Vezzoni, S. (2017). Thallium-rich pyrite ores from the Apuan Alps, Tuscany, Italy: constraints for their origin and environmental concerns. *Miner. Depos.*, 52, 687–707.

Duchesne, J.-C., Rouhart, A., Schoumacher, C., and Dillen, H. (1983). Thallium, Nickel, cobalt and other trace elements in iron sulfides from Belgian lead-zinc vein deposits. *Miner. Depos.*, 18, 303–313.

Gartman, A. and Luther, G. W. (2013.). Comparison of pyrite (FeS_2) synthesis mechanisms to reproduce natural FeS_2 nanoparticles found at hydrothermal sites. *Chem. Geol.*, 120, 447–458.

Gasparrini, M., Bechstadt, T., and Boni, M. (2006). Massive hydrothermal dolomites in the southwestern Cantabrian Zone (Spain) and their relation to the Late Variscan evolution. *Mar. Petrol. Geol.*, 23, 543–568.

Gaudin, A., Mangold, V., Lorand, J.-P., and Pont, S. (2020). Petrogenesis of Tertre Rouge florencite-bearing kaolin deposit, Saint Aubin des Chateaux, Armorican Massif, France. *Ore Geol. Rev.*, 120, article no. 103445.

Gemmell, J. B. and Simmons, S. F. (2007). A group of papers devoted to epithermal Au–Ag deposits. Preface. *Econ. Geol.*, 102(5), 783.

George, L. L., Biagioni, C., Lepore, G. O., Lacalamita, M., Agros, G., Capitani, G. C., Bonaccorsi, E., and d'Acapito, F. (2019). The speciation of thallium in (Tl,Sb,As)-rich pyrite. *Ore Geol. Rev.*, 107, 364–380.

Gloaguen, E., Branquet, Y., Boulvais, P., Moëlo, Y., Chauvel, J. J., Chiappero, P. J., and Marcoux, E. (2007). Palaeozoic oolitic ironstone of the French Armorican Massif: a chemical and structural trap for orogenic base metal-As–Sb–Au mineralisation during Hercynian strike-slip deformation. *Miner. Depos.*, 42, 399–422.

Gloaguen, E., Tourlière, B., and Angel, M. (2016). Revalorisation du potentiel minier français: le district antimonifère du Semnon (Ille et Vilaine-France). Final Report BRGM-62200-FR, BRGM, Orléans. 71 pp.

Griffin, W. L., Powell, W. J., Pearson, N. J., and O'Reilly, S. Y. (2008). GLITTER: data reduction software for laser ablation ICP-MS. *Miner. Ass. Can. Short Course Ser.*, 40, 308–311.

Guillocheau, F. and Rolet, M. (1982). La sédimentation paléozoïque ouest-Armoricaine. *Bull. Soc. Géol. Minéral. Bretagne*, 14, 45–62.

Gumiaux, C., Gapais, D., Brun, J. P., Chantraine, J., and Ruffet, G. (2004). Tectonic history of the Hercynian armorican Shear belt (Brittany, France). *Geodyn. Acta*, 17, 289–307.

Johan, Z., Mantienne, J., and Picot, P. (1974). La routhiérite TlHgAsS3 et la laffittite, AgHgAsS3, deux nouvelles espèces minérales. *Bull. Soc. Fr. Mineral. Cristallog.*, 97, 48–53.

Kaasalainen, A., Stefánsson, A., Giroud, N., and Arnórsson, S. (2015). The geochemistry of trace elements in geothermal fluids, Iceland. *Appl. Geochem.*, 62, 207–223.

Keith, M., Haase, K. M., Klem, R., Krumm, S., and Strauss, H. (2016). Systematic variations of trace element and sulfur isotope compositions in pyrite with stratigraphic depth in the Skouriotissa volcanic-hosted massive sulfide deposit, Troodos ophiolite. *Cyprus. Chem. Geol.*, 423, 7–18.

Kucha, H. and Stumpfl, E. H. (1992). Thiosulfates as precursors of banded sphalerite and pyrite at Bleiberg (Austria). *Mineral. Mag.*, 56, 165–172.

Kucha, H. and Viaene, W. (1993). Compounds with mixed and intermediate sulfur valences as precursors of banded sulfides in carbonate-hosted Zn–Pb deposits in Belgium and Poland. *Miner. Depos.*, 28, 13–21.

Kucha, H., Wouters, R., and Arkens, O. (1989). Determination of sulfur and iron valence by microprobe. *Scanning Microsc.*, 3, 89–97.

Layton-Matthews, D., Leybourne, M. I., Peter, J. M., Scott, S. D., Cousens, B., and Eglington, B. M. (2013). Multiple sources of selenium in ancient seafloor hydrothermal systems: Compositional and Se, S, and Pb isotopic evidence from volcanic-hosted and volcanic-sediment-hosted massive sulfide deposits of the Finlayson Lake District, Yukon, Canada. *Geochim. Cosmochim. Acta*, 117, 313–331.

Le Corre, C., Auvray, B., Ballèvre, M., and Robardet, M. (1991). Le Massif Armoricain. In Piqué, A., editor, *Les massifs anciens de France*, volume 44 of *Sci. Geol. Bull.*, pages 31–103. University Louis Pasteur and Centre National de la Recherche Scientifique, Strasbourg.

Lemarchand, J., Boulvais, P., Gaboriau, M., Boiron, M. C., Tartèse, R., Cokkinos, M., Bonnet, S., and Jégouzo, P. (2012). Giant quartz vein formation and high elevation meteoric fluid infiltration into

the South Armorican Shear Zone; geological, fluid inclusion and stable isotope evidence. *J. Geol. Soc. Lond.*, 169, 17–27.

Lodin, M. (1908). Notice historique sur l'exploitation des mines de Pontpéan (Ille-et-Vilaine). *Ann. Mines*, 10e sér., t. XIV, 5–72.

Lorand, J.-P., Hewins, R. H., Humayun, M., Zanda, B., Remusat, L., La, C., and Pont, S. (2018). Chalcophile-siderophile element systematics of hydrothermal pyrite from martian regolith breccia NWA 7533. *Geochim. Cosmochim. Acta*, 241, 134–149.

Lorand, J.-P., Pont, S., Labidi, J., Cartigny, P., and El Atrassi, F. (2021). Sulphide petrology and contribution of subducted sulphur in diamondiferous garnet-bearing pyroxenites from Beni Bousera (Northern Morocco). *J. Petrol.*, 62, article no. egab089.

Luguet, A., Lorand, J.-P., Alard, O., and Cottin, J. Y. (2004). A multi-technique study of platinum-group elements systematic in some Ligurian ophiolitic peridotites, Italy. *Chem. Geol.*, 208, 175–194.

Maslennikov, V. V., Cherkashov, G., Artemyev, D. A., Firstova, A., Large, R. R., Tseluyko, A., and Kotlyarov, V. (2020). Pyrite varieties at pobeda hydrothermal fields, mid-atlantic ridge 17°07′–17°08′ N: LA–ICP–MS data deciphering. *Minerals*, 10, article no. 622.

Moussu, R. and Prouhet, J. P. (1957). Rapport sur la mine de Pontpéan (Ille-et-Vilaine). BRGM A. 1168 (unpublished report).

Murowchick, J. B. and Barnes, H. L. (1986). Marcasite precipitation from hydrothermal solutions. *Geochim. Cosmochim. Acta*, 50, 2615–2629.

Murowchick, J. B. and Barnes, H. L. (1987). Effect of temperature and degree of supersaturation on pyrite morphology. *Amer. Mineral.*, 72, 1241–1250.

Patten, C. G. C., Pitcairn, I. K., Teagle, D. A. H., and Harris, M. (2016). Mobility of Au and related elements during the hydrothermal alteration of the oceanic crust: implications for the sources of metals in VMS deposits. *Mineral. Deposit.*, 51, 179–200.

Picot, P. and Johan, Z. (1977). Atlas des minéraux métalliques. Bureau des recherches Géologiques et Minières. *Mémoire*, 90, 1–403.

Pillard, F., Chauris, L., and Laforêt, C. (1985). *Inventaire minéralogique de la France.* du BRGM, Paris.

Pochon, A., Beaudoin, G., Branquet, Y., Boulvais, P., Gloaguen, E., and Gapais, D. (2017). Metal mobility during hydrothermal breakdown of Fe–Ti oxides: Insights from Sb–Au mineralizing event (Variscan Armorican Massif, France). *Ore Geol. Rev.*, 91, 66–99.

Pochon, A., Branquet, Y., Gloaguen, E., Ruffet, E. J., Poujol, M., Boulvais, P., Gumiaux, C., Cagnard, F., Baele, J.-M., Kéré, I., and Gapais, D. (2019). Sb ±Au mineralizing peak at 360Ma in the Variscan belt. *Bull. Soc. Géol. Fr. - Earth Sci. Bull,*, 190, article no. 4.

Pochon, A., Gapais, D., Gloaguen, E., Gumiaux, C., Branquet, Y., Cagnard, F., and Martelet, G. (2016a). Antimony deposits in the Variscan Armorican belt, a link with mafic intrusives? *Terra Nova*, 28, 138–145.

Pochon, A., Gloaguen, E., Branquet, Y., Poujol, M., Ruffet, G., Boiron, M. C., Boulvais, P., Gumiaux, C., Cagnard, F., Gouazou, F., and Gapais, D. (2018). Variscan Sb–Au mineralization in central Brittany (France): A new metallogenic model derived from the Le Semnon district. *Ore Geol. Rev.*, 97, 109–142.

Pochon, A., Poujol, M., Gloaguen, E., Branquet, Y., Cagnard, F., Gumiaux, C., and Gapais, D. (2016b). U–Pb LA–ICP–MS dating of apatite in mafic rocks: Evidence for a major magmatic event at the Devonian- Carboniferous boundary in the Armorican Massif (France). *Am. Miner.*, 101, 2430–2442.

Queffurus, M. and Barnes, S.-J. (2015). A review of sulfur-to-selenium ratios in magmatic Nickel–Copper and platinum-group element deposits. *Ore Geol. Rev.*, 69, 301–324.

Rader, S. T., Mazdab, F. K., and Barton, M. D. (2018). Mineralogical thallium geochemistry and isotope variations from igneous, metamorphic, and metasomatic systems. *Geochim. Cosmochim. Acta*, 243, 42–65.

Ramdohr, P. (1980). *The Ore Minerals and Their Intergrowths.* Pergamon, Oxford, 2nd edition.

Reich, M., Deditius, A., Chryssoulis, S., Li, J.-W., Ma, C.-Q., Parada, M. A., Barra, F., and Mittermayr, F. (2013). Pyrite as a record of hydrothermal fluid evolution in a porphyry copper system: a SIMS/EMPA trace element study. *Geochim. Cosmochim. Acta*, 104, 42–62.

Rickard, D. and Luther III, G. W. (2007). Chemistry of Iron Sulfides. *Chem. Rev.*, 107, 514–562.

Ryan, J. G. and Chauvel, C. (2014). The subduction-zone filter and the impact of recycled materials on

the evolution of the mantle. *Treatise Geochem.*, 3, 479–508.

Schoonen, M. A. A. and Barnes, H. L. (1991). Reactions forming pyrite and marcasite fom solution 2. Via FeS precursors below 100 °C. *Geochim. Cosmochim. Acta*, 55, 1505–1514.

Shah, M. T., Ikramuddin, M., and Shervais, J. W. (1994). Behaviour of TI relative to K, Rb, Sr and Ba in mineralized and unmineralized metavolcanics from the Dir area, northern Pakistan. *Miner. Depos.*, 29, 422–426.

Sher, S., Williams-Jones, A. E., and Williams-Jones, G. (2013). Fumarolic activity, acid-sulfate alteration, and high sulfidation epithermal precious-metal mineralization in the crater of Kawah Ijen Volcano, Java, Indonesia. *Econ. Geol.*, 108, 1099–1118.

Smith, I. C. and Carson, B. L. (1977). *Trace Metal in the Environment. Vol. 1. Thallium.* Ann Arbor Science Publishers, Michigan, USA.

Sobbot, R. J., Klaes, R., and Moh, G. H. (1987). Thallium-containing mineral system. Part 1: natural assemblages of Tl-sulfosalts and related laboratory experiments. *Chem. Erde*, 47, 195–218.

Tanon, J. (1961). Rapport sur la mine de La Touche (Ille-et-Vilaine). R BRGM R.5031 (02/61) (unpublished report).

Trautmann, F., Beck-Giraudon, J.-F., and Carn, A. (1994). *Notice explicative de la Feuille Janzé au 1/50000è.* Editions du Service Géologique National. Carte géologique de la France (1/50 000) - Janzé (353). BRGM, Orléans.

Vaughan, D. J. and Craig, J. R. (1978). In Harland, W. B., Cook, A. H., and Hughes, N. F., editors, *Mineral Chemistry of Metal Sulfides*, Earth Science Series, page 493. Cambridge University Press, Cambridge.

Wang, D., Wang, Q., Wang, T., and MSL Science Team (2010). Shape controlled growth of pyrite FeS_2 crystallites via a polymer-assisted hydrothermal route. *Crystal Eng. Commun.*, 12, 3797–3805.

Wilson, S. A., Ridley, W. I., and Koenig, A. E. (2002). Development of sulfide calibration standards for the laser ablation inductively-coupled plasma mass spectrometry technique. *J. Anal. At. Spectrom.*, 17, 406–409.

Zhou, T. F., Fan, Y., Yuan, F., Wu, M. A., Hou, M. J., Voicu, G., Hu, Q. H., Zhang, Q. M., and Yue, S. C. (2005). A preliminary geological and geochemical study of the Xiangquan thallium deposit, eastern China: the world's first thallium-only mine. *Mineral. Petrol.*, 85, 243–251.